Prediction of binary hard-sphere crystal structures

Laura Filion and Marjolein Dijkstra
Soft Condensed Matter, Debye Institute for NanoMaterials Science, Utrecht University, Princetonplein 5, 3584 CC Utrecht, The Netherlands

(Received 13 June 2008; revised manuscript received 25 February 2009; published 30 April 2009)

We present a method based on a combination of a genetic algorithm and Monte Carlo simulations to predict close-packed crystal structures in hard-core systems. We employ this method to predict the binary crystal structures in a mixture of large and small hard spheres with various stoichiometries and diameter ratios between 0.4 and 0.84. In addition to known binary hard-sphere crystal structures similar to NaCl and AlB_2, we predict additional crystal structures with the symmetry of CrB, γCuTi, αIrV, $HgBr_2$, $AuTe_2$, Ag_2Se, and various structures for which an atomic analog was not found. In order to determine the crystal structures at infinite pressures, we calculate the maximum packing density as a function of size ratio for the crystal structures predicted by our GA using a simulated annealing approach.

DOI: 10.1103/PhysRevE.79.046714 PACS number(s): 02.70.−c, 82.70.Dd, 61.46.Hk, 61.50.Ah

I. INTRODUCTION

Close-packed arrangements of hard spheres have been of interest for centuries both as theoretical challenges and as models for various physical systems. However, the question of which structures pack best relies heavily on physical intuition and experimental results. In the case of identical hard spheres, Kepler's 17th century conjecture that the densest arrangement was achieved by stacking close-packed hexagonal planes remained one of the major mathematical challenges until 1998 when Hales presented what appears to be almost a complete proof [1]. However, the prediction of close-packed structures of mixtures of various sized hard spheres is even more challenging due to the enormous size and complexity of the phase space that must be searched to locate the best-packed arrangements. In this paper we use a combination of a genetic algorithm (GA) and Monte Carlo (MC) simulations to search for such crystal structures, attempting to remove much of the (ad-hoc) guess work associated with predicting the crystal structures realized by such systems. By finding the close-packed arrangements, our algorithm predicts crystal structures that are stable at infinite pressures and additionally produces candidate crystal structures for the phase behavior at lower pressures. While most of the structures found for $R_S/R_L<0.6$ [where R_S (R_L) is the radius of the small (large) hard spheres], such as NaCl and AlB_2, have already been discussed in the literature, many of the structures for larger size ratios are novel in the context of the phase behavior of binary hard-sphere mixtures.

The close-packed structures of binary hard-sphere mixtures have been studied intensively as a model for atomic and colloidal systems. In the 1960s Parthé [2] used the concept of packing to explain binary atomic crystal structures found in nature and in 1980 Murray and Sanders argued that binary mixtures of hard spheres order into the structure with the largest possible packing fraction under sedimentation and compaction to explain the long-range crystal structures observed in gem opals [3]. More recently, packing arguments have also been used to explain the experimental observations of intriguing and complicated superlattice structures in binary mixtures of nanoparticles [4,5], of colloidal particles [6–10], and of block copolymer micelles [11]. The underlying idea of these packing arguments is that structures that have a higher close-packed density will have a larger free volume per particle at lower densities, resulting in a higher contribution to the entropy and hence a lower free energy. In studies of self-assembled nanoparticles where non-close-packed crystalline structures are observed it is often asserted that other interactions must play a role [5].

Genetic algorithms, developed first by Holland [12] in the 1970s, provide a framework for finding the optimal solution of a specific problem by mimicking Darwin's principle of "survival of the fittest." GAs enable us to sample efficiently large search spaces in an unbiased and unrestricted way. A basic quantity in a GA [12] is an individual that represents a trial solution to the problem which can be ranked according to a fitness function (e.g., the potential energy). From a random initial population of individuals, the system evolves from generation to generation by using crossover and mutation operators until the population converges to a solution. Originally GAs were designed to search a finite phase space and used a discrete genetic representation of the individuals [12]. Since the 1980s "hybrid" GAs have been widely used to search continuous phase spaces. Such algorithms exploit the advantages of both GAs and local minimizers: a fast local minimization technique is used to relax an individual to its local minimum and mutations and crossovers are employed in the GA to hop between local minima. In this manner continuous parameters, such as the primitive and basis vectors to describe a crystal structure, can be varied to minimize the respective fitness function.

Genetic algorithms were introduced to atomic and molecular systems in the 1990s in an attempt to determine the lowest-energy structure of an atomic cluster [13–15]. Although the first such algorithms involved traditional discrete GAs [13,14], the most commonly used ones are based on a hybrid GA introduced by Deaven and Ho [15]. In their GA the genetic code consists of the atomic positions, and crossovers are performed by cutting clusters with a plane in real space; the complementary partial spaces are recombined from parent clusters and the resulting structures relaxed to their local minimum with a conjugate gradient algorithm. Variations in this technique have since been used to study

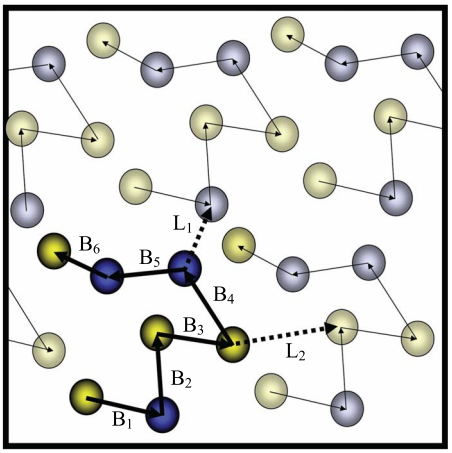

FIG. 1. (Color online) A typical 2D "hydra" for a binary system with seven particles in the unit cell: three of type A (darker spheres) and four of type B (lighter spheres).

many clusters, however, the use of GAs to study periodic systems such as colloidal and atomic systems is much more recent and employ either a lattice and basis representation of the crystal structure [16,17], a discrete binary representation of these vectors [18], or a so-called "hydra" representation based on displacement vectors [19]. A cartoon of the hydra representation is depicted in Fig. 1. This last implementation has been applied to a system with approximately hard interactions. The inclusion of hard interactions in a GA complicates the problem severely as most crossover and mutation operations cause particle overlap. Many forbidden regions are present in the search space that should be circumvented. In this paper, we use a modification of the GA based on the hydra representation to search for close-packed structures in binary hard-sphere systems.

This paper is organized in the following manner. In Sec. II we describe the method we used to determine the binary crystal structures, including a description of the GA. In Sec. III we present a table with the structures we have found along with space filling curves for the best-packed structures with AB and AB_2 stoichiometry. Finally, in Sec. IV we discuss the results and our conclusions.

II. METHOD

In this paper we employ a combination of a GA and Monte Carlo simulations to maximize the packing fraction of a binary crystal structure for a given stoichiometry and particle radius ratio α (R_S/R_L). The GA we use is based on the algorithm introduced by Stucke and Crespi [19] to examine ternary hard-sphere systems. As the packing fraction depends only on the volume of the unit cell and not on the basis vectors, the algorithm will encounter severe convergence problems if the packing fraction is used as the fitness function. Hence, the packing fraction is not a suitable fitness function for a hybrid GA. The method proposed by Stucke and Crespi attempts to avoid this problem by minimizing a fictitious potential. We follow a similar route here but extend the approach as follows: we first use a GA to locate the

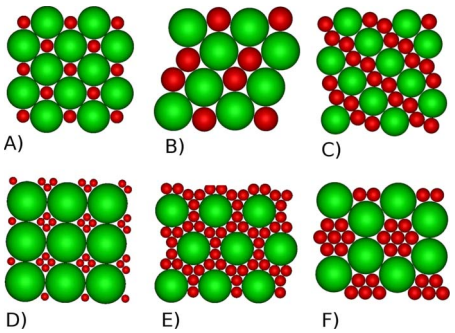

FIG. 2. (Color online) 2D crystal structures predicted using the GA. The naming convention for the crystal structures is consistent with Ref. [21]. (A) crystal structure S_1: AB stoichiometry with α=0.4, (B) H_2: AB, α=0.63, (C) H_1: AB_2, α=0.54, (D) S_2: AB_4, α=0.2, (E) T_2: AB_6, α=0.34, (F) H_3: A_2B_7, α=0.38.

energy minima of a fictitious potential for a certain size ratio and stoichiometry. Subsequently, we employ the lowest-energy structures as candidate structures for the best-packed crystal structures for binary hard-sphere mixtures. As the optimized structure for the fictitious potential does not have to correspond with the best-packed structure for the hard-sphere mixtures at the same size ratio, we replace the fictitious potential with a true hard-sphere interaction, expand the unit cell until any resulting overlaps are removed, and then use a Monte Carlo pressure annealing simulation to crush the resulting structure to the best packing. The structure is then identified either by inspection, or with the FINDSYM program [20]. We wish to make a few remarks here: (i) as the fictitious potential that we employ consists of a very steeply repulsive, nearly hard-sphere-like potential, and a very short-range attractive tail, we did not encounter any numerical accuracy problems in resolving the energy minima using the GA. (ii) Our method is based on the conjecture that the lowest-energy structures using the fictitious potential correspond to the best-packed structures for the hard-sphere systems, which is not obvious and cannot be proven rigorously. However, if we apply our method to two-dimensional (2D)

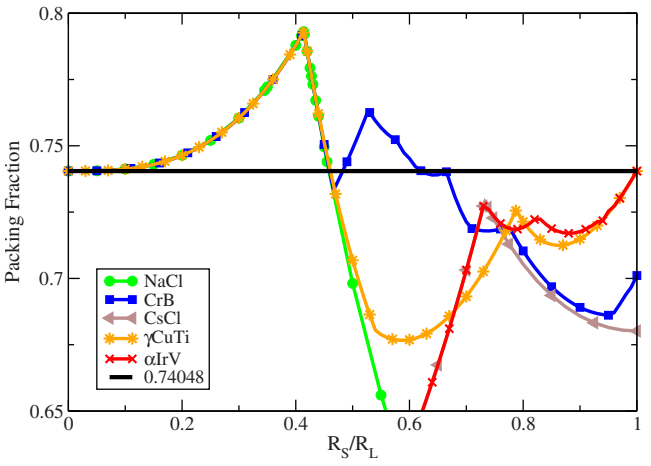

FIG. 3. (Color online) Space filling curves for the AB structures listed in Table I. Only a fraction of the data points were plotted to simplify the image.

and three-dimensional (3D) hard-core systems, which have been previously examined [21,22], we find perfect agreement in all cases, thereby providing confidence in our method. A more detailed description about these results will be given in Sec. III. In conclusion, the GA with a fictitious potential is used to find the lowest-energy crystal structures, which serve as candidate crystal structures for the best-packed structures of binary hard-sphere mixtures. We perform Monte Carlo pressure annealing simulations to find the best packing of the candidate structures as a function of size ratio.

A. Genetic algorithm

An individual in our GA is a system representation for a crystal structure. As mentioned in Sec. I, we have chosen to represent crystal structures using a displacement vector representation, called the "hydra" representation [19]. A cartoon illustrating the "hydra" representation is shown in Fig. 1. In our version of the "hydra" representation the genetic code consists of two sequences, one for the basis particles and one for the periodic lattice. In d dimensions with N distinguishable particles per unit cell, the first sequence consists of the displacement vectors between particles and is given by the hydra $\mathbf{B}=\mathbf{B}_1,\mathbf{B}_2,\ldots,\mathbf{B}_{N-1}$. The vector $\mathbf{B}_i$ connects particle i to $i+1$ in this representation. In the hydra representation the particles connected by the displacement vectors are generally not in the same unit cell, however, there is exactly one image of each particle in the hydra. The second sequence contains the lattice vectors of the hydra $\mathbf{L}=\mathbf{L}_1,\ldots,\mathbf{L}_d$, which denote the projections to periodic images of the hydra. We note that $\mathbf{L}_i$ can interconnect a particle with its image, but it can also interconnect distinct particles in the hydra. The particles that are interconnected by the lattice vectors $\mathbf{L}_i$ are selected at the beginning of the GA. To initialize a hydra, the displacement vectors $\mathbf{B}_i$ are chosen according to a Gaussian distribution peaked at $1.2(R_i+R_{i+1})$, where R_i denotes the radius of particle i. The angular orientation is then chosen at random. The lattice vectors $\mathbf{L}_i$ are chosen in the same manner. We start our GA with a random initial population of hydras.

In theory we would like to use the packing fraction as a fitness function, but in that case the GA experiences convergence problems as the packing fraction is independent of the particle positions in the cell. Instead, we replace the hard-sphere interaction by the following pair potential:

$$V(r_{ij}) = \epsilon_{ij}\left[\left(\frac{\sigma_{ij}}{r_{ij}}\right)^m - \left(\frac{\sigma_{ij}}{r_{ij}}\right)^n\right], \tag{1}$$

where r_{ij} is the interparticle distance between particles i and j. The parameter σ_{ij} was chosen such that the corresponding hard particles with respective radii $R_{i(j)}$ are in contact but not overlapping at the minimum of the potential, thus,

$$\sigma_{ij} = (R_i + R_j)\left(\frac{m}{n}\right)^{1/(n-m)}. \tag{2}$$

The fitness function is then the sum of these pairwise interactions. As this is now a continuous function of all lattice parameters, the local minima can easily be determined using a conjugant gradient method. In our implementation of the algorithm, we have typically chosen $m=42$ and $n=24$ in the pairwise potential, however, we have checked for various stoichiometries and size ratios that other values of n result in the same crystal structures implying that our results are robust with respect to the fictitious attractive tail. Additionally, we have also tested the robustness of this method by applying our method to 2D and 3D systems, which have been previously examined [21,22], and we find agreement for all cases and conclude that the softness of the potential did not change the results.

The genetic algorithm starts with a population of M members. To search space more efficiently, each hydra is relaxed to its local minimum using the Broyden-Fletcher-Goldfarb-Shanno (BFGS) algorithm [23]. In the hydra representation, the potential-energy calculation can be computationally expensive as it is possible that several images must be summed over before all the interactions within the cutoff radius of a single hydra are included. For instance, it is possible that some of the nearest neighbors of a particle in a given hydra are several lattice vectors away. In a Bravais representation, however, it is possible to determine in advance the number of cells along each lattice vector that are needed to calculate the potential energy of a crystal structure. It is thus advantageous to map the hydra to a Bravais representation before relaxing the structure. For this purpose the Bravais lattice vectors are constructed from the $\mathbf{L}$ vectors and a lattice reduction algorithm is used to produce a more cubic unit cell. In 2D we use the well-known Gaussian reduction algorithm while in 3D we use the lattice reduction method described in Ref. [18]. The 3D method attempts to minimize the surface area of the unit cell. Denoting the lattice vectors $\mathbf{r}_1,\mathbf{r}_2,\mathbf{r}_3$ and the surface area of the box spanned by the vectors A, the 12 linear combinations,

$$\mathbf{r}_i^{\text{new}} = \mathbf{r}_i \pm \mathbf{r}_l, \tag{3}$$

with $i \neq l \in \{1,2,3\}$, are determined and the surface areas $A_{i,l}^{\text{new}}$ of the new boxes spanned by $\mathbf{r}_i^{\text{new}}$, $\mathbf{r}_j$, $\mathbf{r}_k$ are compared to A. If any of the $A_{i,l}^{\text{new}}$ is smaller than A than the corresponding $\mathbf{r}_i$ is set to $\mathbf{r}_i^{\text{new}}$, otherwise the algorithm terminates. A single hydra is then mapped to the resulting unit cell and relaxed to its local minima. The hydra representation is then reconstructed in the following manner: the $\mathbf{B}_i$'s are found by taking the shortest vector between any image of particle i and $i+1$ and the $\mathbf{L}_i$'s are constructed similarly. The mapping between the hydra and Bravais representations is one of the main differences between our algorithm and the one in [19] where the potential energy is calculated by summing *all* the interactions between W^d hydras with d the dimensionality. Our mapping between the hydra and Bravais representations serves two purposes. First, for the energy calculation the number of cells which need to be summed over is less than or equal to the W^d boxes summed in Ref. [19], and hence significantly faster. Second, neighbors in the hydra representation remain close in real space. This increases the speed of the local minimization and prevents displacement vectors from becoming exceedingly long. Additionally, according to the building block hypothesis for GAs, having the most related parameters close in the system representation improves the GA convergence [24].

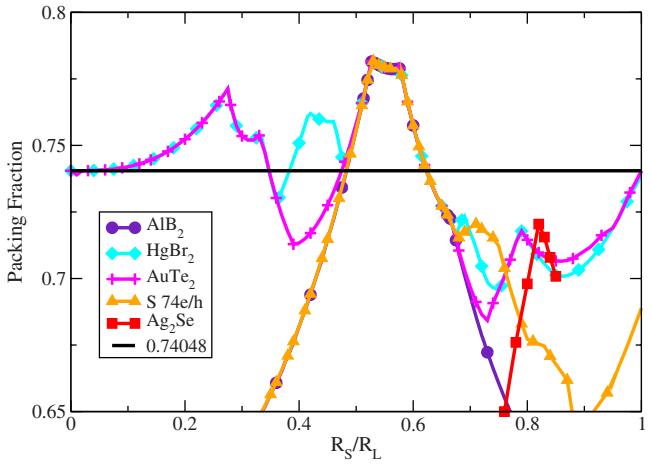

FIG. 4. (Color online) Space filling curves for the AB_2 structures listed in Table I.

A new generation consists of S offspring produced by mutations and crossovers. To produce an offspring, two parents are selected at random (denoted p_1 and p_2) from the current generation. Each displacement vector in the corresponding **B**'s undergoes a random mutation in its length with a probability of 10%. The first step in the crossover is to randomly choose a k_1 between 0 and d. The first k_1 vectors of the sequence L are then taken from p_1 and the remaining from p_2. The new lattice vectors are tested to make sure that they are not colinear. If they are then a new k_1 is chosen. Next a random crossover point k_2 is chosen between 1 and $N-2$. The first k_2 elements of the sequence **B** are then taken from p_1 and the rest from p_2. The two partial hydra are then rotated in real space around the connection point until a minimum in the potential energy is found. The structure is then relaxed to its local minimum as previously described. For the candidate structure to become a member of the offspring it must still meet three additional requirements: that (i) the bond lengths are less than some maximum value r_{max}, that (ii) its fitness is better that the worst of the previous generation and that (iii) its normalized dot product with the members of the current generation and any other current offspring is less than 0.8. The latter requirement is needed to prevent the offspring from being located in the same local minima as the other members, and allows us to work with a rather small population. However, if the normalized dot product between the potential offspring and a single member is greater than 0.80 and if the fitness is better it replaces the other. The bond-length restriction is used to select out a specific set of solutions. For instance, for large R_S/R_L ratios, the best-packed solution is always phase separated hexagonal-close-packed structures of small and large hard spheres. However, by restricting the bond lengths, we are able to exclude this possibility and force the simulation to find the next best solution. Since we are interested in binary hard-sphere crystal structures, this is an essential component of the algorithm. It should be noted, however, that this restriction is only important for larger unit cells (with ≈ 8 or more colloids per unit cell). When S children are produced in this way, the next generation is produced by a form of elitism where the best M members of the parents and offspring are

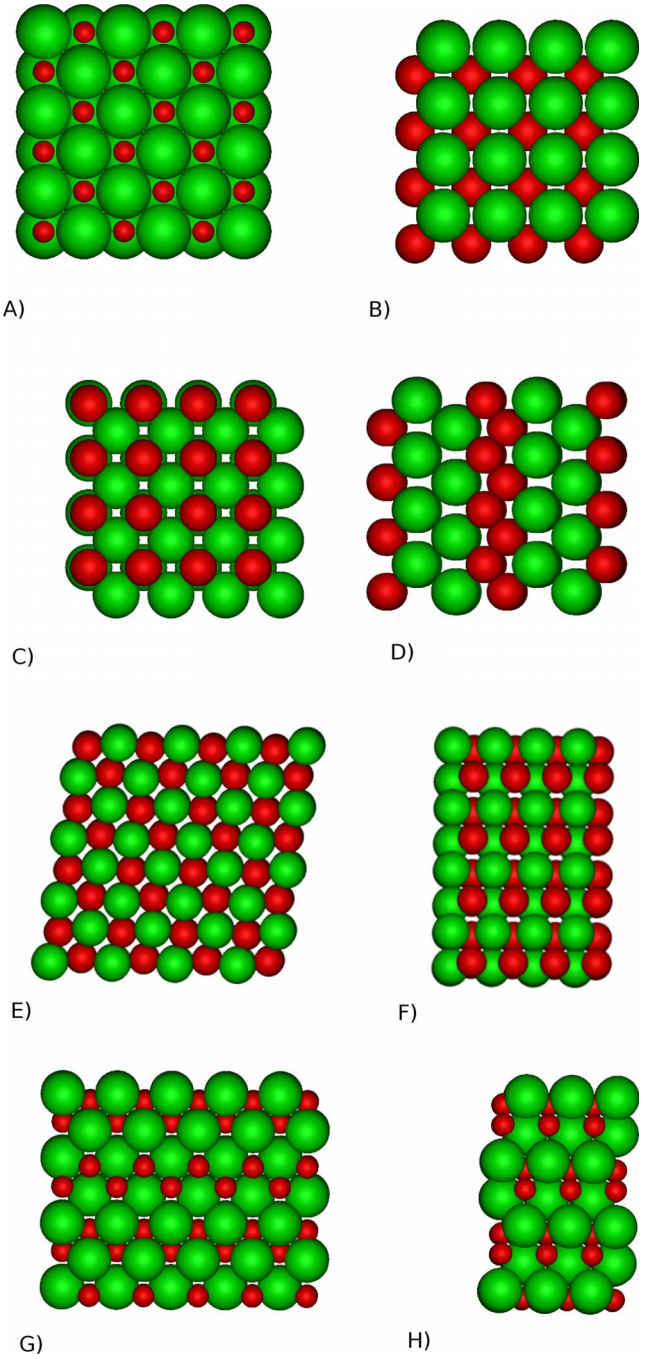

FIG. 5. (Color online) Cartoons of the AB crystal structures which have the best overall packing for a given size ratio. (A) NaCl, $\alpha=0.4$, (B) CsCl, $\alpha=0.73$, [(C) and (D)] γCuTi, $\alpha=0.8$, xy, and xz planes, respectively, [(E) and (F)] αIrV, $\alpha=0.82$, xy, and xz planes [(G) and (H)] CrB, $\alpha=0.6$ xy and xz.

taken. The algorithm terminates when all the members of the population have the same energy (within δE) for 10–20 generations. In the majority of our simulations we used $M=20$ and $S=10$. If either M or S are much larger, than the normalized dot product restriction is rarely met and many candidate structures are thrown out. In summary, our modifications to the GA, which improved significantly the speed and convergence of the algorithm, allowed us to systematically predict

TABLE I. Binary crystal structures with the largest packing fraction predicted for various α ratios for AB (4), AB_2 (6), AB_3 (4), AB_4 (5), AB_5 (6) and AB_6 (7) stoichiometries where the number in ( ) refers to the number of colloids per unit cell studied. * was calculated with 12 colloids per unit cell and in addition to Ag_2Se another structure was found, which is a distortion of the $MgZn_2$ Laves phase, but with extremely low symmetry and a packing of 0.716.

α	0.4	0.5	0.6	0.7
AB	NaCl/NiAs	CrB	CrB	CrB
	0.788	0.749	0.745	0.722
AB_2		$AuTe_2$	AlB_2	S 74h/e
		0.756	0.757	0.718
AB_3	S 5b/ac	S 19b/1f	S 12 c/ib	S 8a/aaa
	0.722	0.744	0.721	0.672
AB_4	S 1a/aaaa	S 160a/ab	S 123d/fg	S 38b/de
	0.738	0.725	0.737	0.666
AB_5		S 8a/abb	S 8a/bba	S 183a/bc
		0.690	0.713	0.690
AB_6	S 10d/gj	S 83c/gk	S 38a/dee	S 69b/ij
	0.756	0.710	0.729	0.680
α	0.72	0.74	0.76	0.78
AB	CsCl	CsCl	CrB	CrB
	0.719	0.726	0.719	0.718
AB_2	SG 74h/e	SG 74h/e	SG 74h/e	$AuTe_2/HgBr_2$
	0.719	0.715	0.704	0.714
AB_3	S 12d/ai	S 12d/ai	S 12c/ib	S 6b/aab
	0.672	0.670	0.669	0.684
AB_4	S 65b/ij	S 65d/ij	S 65d/gh	S 65c/gh
	0.664	0.655	0.647	0.640
AB_5	S 183a/bc	S 183a/bc	S 160a/aab	S 189a/cg
	0.688	0.686	0.674	0.684
α	0.8	0.82	0.84	
AB	γCuTi	αIrV	αIrV	
	0.721	0.722	0.729	
AB_2	$AuTe_2$	Ag_2Se^*	$AuTe_2$	
	0.714	0.7204	0.707	
AB_3	S 123b/ah	S 12d/ai	S 47b/al	
	0.694	0.672	0.700	
AB_4		S 87b/h	S 87b/h	
	0.698	0.705	0.704	
AB_5	S 189a/cg	S 183 b/df	S 8 a/abb	
	0.688	0.686	0.667	
AB_6	S 139b/ge	S 2	S 12a/iii	
	0.658	0.674	0.695	

candidate crystal structures for a large range of size ratios and stoichiometries and to locate binary crystal structures even when monodisperse (rHCP) crystal structures pack better.

B. Monte Carlo pressure annealing

The GA in Sec. II A minimizes a fictitious potential. Replacing the fictitious pair potential from the previous algorithm with a hard-sphere potential often results in either slight overlaps of the particles or holes in the structure. Thus, in order to find the true, hard-sphere packing fraction of the resulting structure, an additional method is needed. To solve this problem we employ a form of MC pressure annealing. The "hydra" representation is first mapped to its corresponding Bravais lattice. The resulting lattice vectors are used as the simulation box. In this MC simulation, a typical Metropolis algorithm is used to move particles in a unit cell, while volume moves allow both the size and the shape of the simulation box to vary. An initial pressure is chosen such that the crystal structure cannot melt and the pressure is slowly increased until the particles can no longer move (to single precision accuracy). This pressure is higher for particles with small R_S/R_L values as they melt at lower pressures. The resulting structure is then identified either by inspection, or with the FINDSYM program [20].

III. METHOD VERIFICATION AND RESULTS

To test the algorithm we have examined various systems of hard disks and hard spheres with up to 20 particles per unit cell. In 2D monodisperse systems we found hexagonal lattices and in 3D the GA converged to crystal structures consisting of stacked hexagonal planes in face-centered-cubic (FCC), hexagonal-close-packed (HCP) and rHCP arrangements as conjectured by Kepler. In all cases the GA converged to several different hydra representations of the same crystal structures suggesting that the potential minimum was indeed found. We also examined 2D binary systems with AB, AB_2, AB_4, AB_6, and A_2B_7 stoichiometries for various size ratios, a system examined previously by Likos and Henley [21]. Our results are shown in Fig. 2 and agree with their predictions. It should be noted that we did not do an extensive search of the phase space, but rather used this as a check of the algorithm. The stoichiometries we checked were chosen to be representative of their results. However, it is still possible that a more thorough study of the binary hard disk system would yield new structures. Additionally, unlike the algorithm we used, the method of Likos and Henley involved systematically filling holes in the lattice of typical monodisperse 2D lattices with smaller particles and allowing the crystalline structures to distort in a manner that resulted in best packings for the given size ratio and stoichiometry. However, unlike our search, the method used by Likos and Henley [21] relied on preselected structures for their searches while the GA implementation used here searches all possible binary crystals with the only restriction being the number of particles per unit cell.

Additionally, we studied binary mixtures in 3D with AB [25], AB_2 AB_3, AB_4, AB_5, and AB_6 stoichiometries for various size ratios. The structure with the densest packing fraction had either AB or AB_2 stoichiometry for any given size ratio. Our results for all stoichiometries are summarized in Table I.

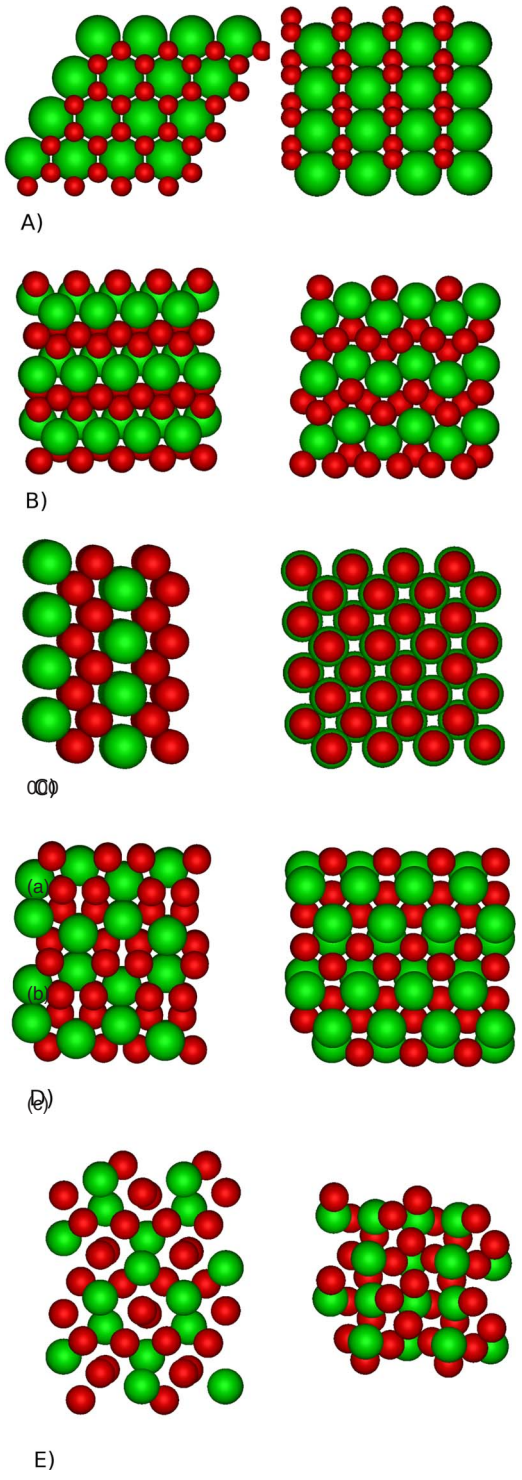

FIG. 6. (Color online) Cartoons of the AB_2 crystal structures which have the best overall packing for a given size ratio. (A) AlB_2, α=0.6, (B) $HgBr_2$, α=0.69, (C) $AuTe_2$, α=0.78 (D) S74e/h, α =0.72 (E) $AgSe_2$, α=0.82.

The crystal structures are identified by an atomic analog of the binary structure which has the same space group and Wyckoff positions. For instance, $AuTe_2$ refers to a structure which has the symmetry associated with space group 12 when the 2a Wyckoff positions are occupied by the larger particles and the 4i positions are occupied by the smaller

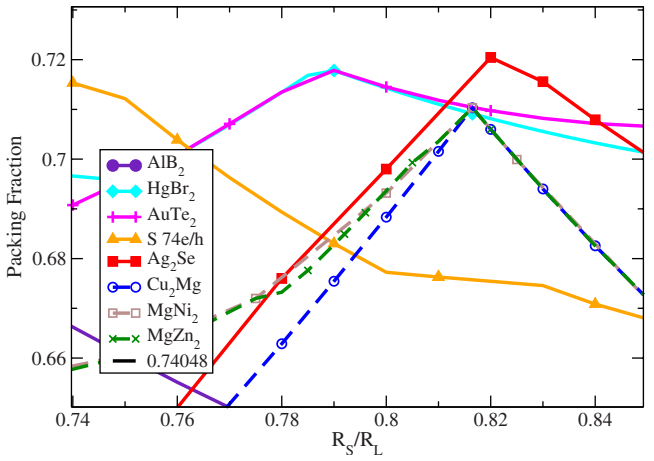

FIG. 7. (Color online) Space filling curves for the AB_2 structures listed in Table I compared with the Laves phases.

particles, this leaves 6 degrees of freedom for the structure (a,b,c,β,x,z). Hence, structures which have been identified as $AuTe_2$ may have different lattice parameters. When no atomic analog was found the structures were listed by their space group and occupied Wyckoff positions.

In order to determine the best-packed crystal structures for a given size ratio, we calculate the space filling curves for all the AB and AB_2 structures predicted by our GA. To this end, we maximize, for a given structure and size ratio, the packing fraction as a function of the lattice parameters using a simulated annealing algorithm. For a given structure and size ratio, the packing fraction was maximized as a function of the lattice parameters using a simulated annealing algorithm. Since the number of free parameters describing a given structure is typically small, it is often possible to maximize the packing fraction for the hard-sphere potential [26]. The space filling curves of the AB and AB_2 structures listed in Table I are shown in Figs. 3 and 4, and specific data points which can be used to reproduce the plots is given in Table II. Cartoons depicting the associated crystal structures are shown in Figs. 5 and 6. For comparison with our results, we have also included the space filling curves of the Laves

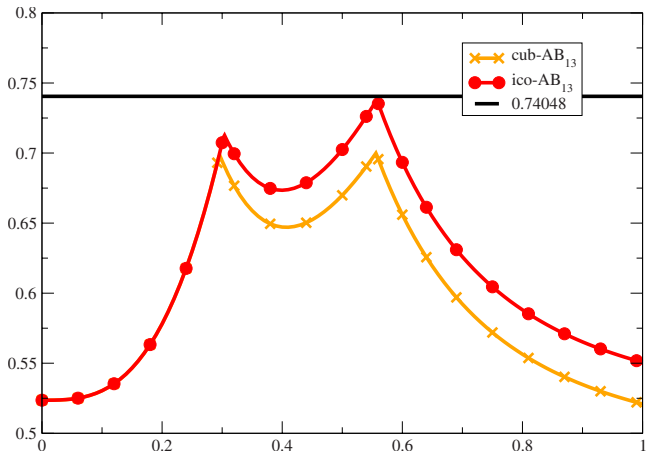

FIG. 8. (Color online) Space filling curves for the cuboctahedral and icosahedral AB_{13} crystal structures.

TABLE II. Maximum packing fraction for the AB and AB_2 crystal structures as a function of the size ratio α.

α	Ag_2Se	S 74e/h	$HrBr_2$	AlB_2	$AuTe_2$	CsCl	γCuTi	NaCl	CrB	αIrV
0.000		0.605	0.741	0.605	0.741	0.524	0.741	0.741	0.741	
0.050		0.605	0.741	0.605	0.741	0.524	0.741	0.741	0.741	
0.100		0.606	0.742	0.606	0.742	0.524	0.741	0.741	0.741	
0.150		0.609	0.746	0.609	0.746	0.525	0.743	0.743	0.743	
0.200		0.614	0.752	0.614	0.752	0.528	0.746	0.746	0.746	
0.250		0.624	0.764	0.624	0.764	0.532	0.752	0.752	0.752	
0.275			0.771		0.771					
0.300		0.637	0.754	0.637	0.754	0.538	0.761	0.761	0.761	
0.333			0.754							
0.330					0.754					
0.350		0.656	0.738	0.656	0.738	0.546	0.772	0.772	0.772	
0.362			0.729							
0.390					0.713					
0.400		0.682	0.751	0.682	0.713	0.557	0.788	0.788	0.788	
0.414							0.793	0.793	0.793	
0.418			0.762							
0.450		0.715	0.759	0.715	0.728	0.571	0.751	0.750	0.751	
0.461			0.759							
0.480			0.744							
0.466									0.734	
0.500		0.756	0.758	0.756	0.758	0.589	0.707	0.698	0.749	
0.527									0.763	
0.528		0.781	0.781	0.782	0.782					
0.550		0.779	0.779	0.779	0.779	0.611	0.679	0.656	0.757	
0.575									0.752	
0.577				0.779						
0.578		0.778	0.778		0.778					
0.600		0.758	0.758	0.758	0.758	0.637	0.677	0.622	0.745	
0.650		0.727	0.727	0.727	0.727	0.667	0.682	0.594	0.739	0.667
0.665			0.723	0.722	0.722				0.740	
0.675			0.716							
0.680		0.716								
0.690			0.723							
0.700		0.719	0.717	0.693	0.697	0.703	0.693	0.573	0.721	0.703
0.710		0.721								
0.720	0.620									
0.726					0.684					
0.733						0.729				
0.735										0.728
0.750	0.639	0.712	0.696	0.661	0.696	0.722	0.710	0.556	0.718	0.723
0.775									0.720	
0.788			0.718				0.726			
0.790					0.718					
0.800	0.698	0.677	0.714	0.637	0.715	0.705	0.721	0.543	0.710	0.719
0.820	0.720									
0.825										0.723
0.830		0.675								
0.850	0.701	0.668	0.701	0.622	0.707	0.694	0.713	0.534	0.697	0.719

TABLE II. (*Continued.*)

α	Ag_2Se	S 74e/h	$HrBr_2$	AlB_2	$AuTe_2$	CsCl	γCuTi	NaCl	CrB	αIrV
0.870		0.662								
0.900		0.645	0.705	0.612	0.710	0.686	0.715	0.528	0.689	0.718
0.950		0.661	0.719	0.606	0.719	0.682	0.725	0.525	0.686	0.725
1.000		0.689	0.741	0.605	0.741	0.680	0.741	0.524	0.701	0.741

phases in Fig. 7 as well as the cuboctahedral (cub) and icosahedral (ico) AB_{13} in Fig. 8. In the case of the AB_{13} structures, the only parameter varied was the overall lattice scaling.

IV. DISCUSSION AND CONCLUSIONS

From the packing fraction curves it is possible to predict the infinite pressure phase diagrams since, for a given size ratio α, the structure with the largest packing fraction is stable at infinite pressures. Hence we predict NaCl/NiAs ($0 < \alpha \leq 0.44$), $HgBr_2$ (0.44–0.48), $AuTe_2$ (0.48–0.53), and AlB_2 (0.53–0.62). For size ratios larger than 0.62 monodisperse FCC/HCP/rHCP have the largest packing.

In contrast, at finite pressures, it is necessary to compare the Gibbs free energies to determine the stability of a phase. To date, such analyses on binary hard-sphere systems have included NaCl (stable for $0.2 < \alpha < 0.42$), AlB_2 (0.42–0.59), $icoAB_{13}$ (0.48–0.62), CsCl (no known stable region), and the Laves phases (0.74–0.84) [27–32]. Many of these calculations were motivated by experimental evidence for these structures in approximately hard-sphere systems, as well as the fact that they all pack well at some size ratio. The packing fractions of these structures are shown in Figs. 3, 4, 7, and 8. Experimentally, AlB_2 and $icoAB_{13}$ have been seen in a large variety of systems, including gem opals [3], approximately hard colloidal systems [8,9], and more recently in nanoparticles [5,33]. NaCl, NiAs, the Laves phases, and CsCl have also been seen experimentally in colloidal systems [8,34–36] and nanoparticle systems [5]. While the question remains whether these experimentally realized particles interact with truly a hard-core interaction, these structures nonetheless present a reasonable starting place for finite pressure calculations.

While the Laves phases were predicted to be stable for a finite pressure region when $\alpha = 0.82$ [32], in Fig. 7 we see that the Laves phases are not the best-packed candidates. Instead, at $\alpha = 0.82$ we find a number of structures which pack better than the Laves phases, including αIrV, γCuTi, $AuTe_2$, and Ag_2Se. Full free-energy calculations show that the only stable structures at this size ratio are the Laves phases [37]. Additionally, constant pressure NPT MC simulations show that Ag_2Se melts into $MgCu_2$ at pressures where the more symmetric $MgCu_2$ is predicted to be stable. Thus, Ag_2Se can be looked at as a high-pressure distortion of $MgCu_2$. Hence, at a size ratio of 0.82 the binary hard-sphere system seems to favor the more symmetric crystal structure over the best-packed structure. As a result, the space filling arguments currently being used to explain the crystal structures of nanoparticles, specifically, studies such as [5], which make the direct association of the entropic contribution to the free energy with the space filling curves, are not always valid.

In contrast, while $icoAB_{13}$ packs better then $cubAB_{13}$, as shown in Fig. 8, NPT MC simulations show that the more symmetric $cubAB_{13}$ melts into $icoAB_{13}$ for the size ratio range where $icoAB_{13}$ is predicted to be stable. In this case it appears that the system chooses the lower symmetry, higher packed crystal structure in agreement with the space filling arguments. However, in this case, the result violates the symmetry principle proposed by Laves in 1956 [38], which states that the structure with the highest symmetry is adopted.

Taken together, these results imply that when examining the phase behavior of systems at finite pressures it is important to examine *both* the close-packed structures and the related higher symmetry crystal structures. While it is possible that this behavior is simply due to the particle free volume not scaling with the unit cell volume, the fact that the system (as in the case of the Laves phases) sometimes chooses the lower packed, higher symmetry structures indicates that lattice vibrations may be important in the phase behavior of binary hard-sphere crystal structures. Our results also show that there are a number of additional structures, particularly for $\alpha > 0.6$, not previously studied in the context of binary hard-sphere mixtures which may be stable for binary hard-sphere systems. Moreover, as the structures stable for hard spheres are also seen in systems with soft interactions, for instance NaCl, AlB_2, and $icoAB_{13}$, and the Laves phases have been seen in nanoparticle systems [4,5] and $icoAB_{13}$ was seen in block copolymer micellar systems [11], the predicted structures can also be used as a starting point for phase behavior studies of many such systems.

In conclusion, we have used a combination of a GA, MC NPT simulations, and simulated annealing techniques to predict close-packed binary hard-sphere crystalline structures for a wide range of stoichiometries and sphere diameter ratios. The results are in agreement with the known structures and show that there are a number of as yet unexamined binary crystal structures with competing packing fractions for α between 0.6 and 0.84. Additionally, our results demonstrate the importance of full Gibbs free-energy calculations in determining the stability of binary crystal structures indicating that the association of the entropic free-energy contribution to the packing fraction is not always valid. Finally, we

stress that our GA and NPT MC simulations can easily be extended to find crystal structures for multicomponent mixtures, particles with soft interactions, and nonspherical particles.

ACKNOWLEDGMENTS

This work was financially supported by the High potential program of Utrecht University.

[1] T. C. Hales, Ann. Math. **162**, 1065 (2005).
[2] E. Parthé, Z. Kristallogr. **115**, 52 (1961).
[3] M. J. Murray and J. V. Sanders, Philos. Mag. A **42**, 721 (1980).
[4] F. Redl *et al.*, Nature (London) **423**, 968 (2003).
[5] Z. Chen, and S. O'Brien, ACS Nano **2**, 1219 (2008), and references therein.
[6] K. P. Velikov *et al.*, Science **296**, 106 (2002).
[7] M. E. Leunissen *et al.*, Nature (London) **437**, 235 (2005).
[8] N. Hunt, R. Jardine, and P. Bartlett, Phys. Rev. E **62**, 900 (2000).
[9] A. B. Schofield, P. N. Pusey, and P. Radcliffe, Phys. Rev. E **72**, 031407 (2005).
[10] P. Bartlett, R. H. Ottewill, and P. N. Pusey, Phys. Rev. Lett. **68**, 3801 (1992).
[11] S. Abbas and T. P. Lodge, Langmuir **24**, 6247 (2008).
[12] J. H. Holland, *Adaption in Natural and Artifical Systems* (MIT Press/Bradford Books Editions, Cambridge, MA, 1992).
[13] Y. Xiao and D. E. Williams, Chem. Phys. Lett. **215**, 17 (1993).
[14] B. Hartke, J. Phys. Chem. **97**, 9973 (1993).
[15] D. M. Deaven and K. M. Ho, Phys. Rev. Lett. **75**, 288 (1995).
[16] A. R. Oganov and C. W. Glass, J. Chem. Phys. **124**, 244704 (2006).
[17] N. L. Abraham and M. I. J. Probert, Phys. Rev. B **73**, 224104 (2006).
[18] D. Gottwald *et al.*, J. Chem. Phys. **122**, 204503 (2005).
[19] D. P. Stucke and V. H. Crespi, Nano Lett. **3**, 1183 (2003).
[20] H. T. Stokes, D. M. Hatch, and B. J. Campbell, ISOTROPY, stokes.byu.edu/isotropy.html, (2007).
[21] C. N. Likos and C. L. Henley, Philos. Mag. B **68**, 85 (1993).
[22] J. K. Kummerfeld, T. S. Hudson, and P. Harrowell, J. Phys. Chem. B **112**, 10773 (2008).
[23] J. N. R. H. Byrd, P. Lu, and C. Zhu, SIAM J. Sci. Comput. (USA) **16**, 1190 (1995).
[24] D. E. Goldberg, *Genetic Algorithms in Search Optimization and Machine Learning* (Addison-Wesley Publishing, Reading, MA, 1989).
[25] Additionally, since the first submission of this work, a paper predicting 3D binary hard-sphere crystal structures with AB stoichiometries has been published [22]. We have additionally compared out results for 3D AB stoichiometry with this paper and found agreement. Ref. [25] examined the packing of known inorganic binary crystalline structures using a simulated annealing approach.
[26] In the case of Ag_2Se however, the structure has 12 internal parameters and the simulated annealing approach only worked when a good initial guess was known. Hence, near 0.82 we were able to use the structure predicted by the GA, but we were unable to determine the packing for the full set of size ratios.
[27] M. D. Eldridge *et al.*, Nature (London) **365**, 35 (1993).
[28] E. Trizac *et al.*, Mol. Phys. **90**, 675 (1997).
[29] M. D. Eldridge *et al.*, Mol. Phys. **79**, 105 (1993).
[30] X. Cottin and P. A. Monson, J. Chem. Phys. **102**, 3354 (1995).
[31] A. R. Denton and N. W. Ashcroft, Phys. Rev. A **42**, 7312 (1990).
[32] A.-P. Hynninen *et al.*, Nature Mater. **6**, 202 (2007).
[33] K. Overgaag *et al.*, J. Am. Chem. Soc. **130**, 7833 (2008).
[34] A. B. Schofield, Phys. Rev. E **64**, 051403 (2001).
[35] S. Yoshimura and S. Hachisu, Prog. Colloid Polym. Sci. **68**, 59 (1983).
[36] E. C. M. Vermolen *et al.*, Fabrication of large binary colloidal crystals with a NaCl-structure (to be published).
[37] A.-P. Hynninen, and L. C. Filion, and M. Dijkstra, Stability of LS and LS_2 crystal structures in binary mixtures of hard and charged spheres (to be published).
[38] F. Laves, *Theory of Alloy Phases* (American Society for Metals, Metals Park, Ohio, 1956).